

See discussions, stats, and author profiles for this publication at: <https://www.researchgate.net/publication/258683411>

Lamellar Orientation Inversion under Dynamic Interplay between Crystallization and Phase Separation

ARTICLE *in* MACROMOLECULES · JANUARY 2012

Impact Factor: 5.8 · DOI: 10.1021/ma202046c

CITATIONS

20

READS

31

6 AUTHORS, INCLUDING:



[Yongri Liang](#)

Beijing Institute of Petrochemical Technology

46 PUBLICATIONS 408 CITATIONS

[SEE PROFILE](#)

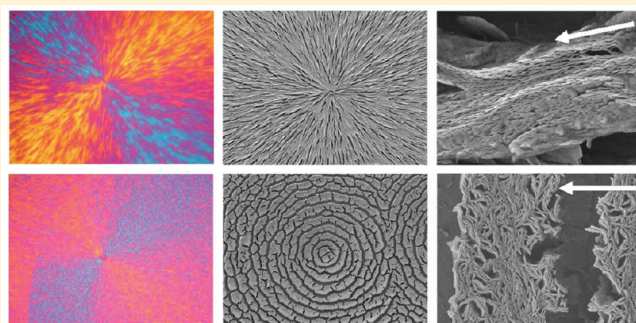
Lamellar Orientation Inversion under Dynamic Interplay between Crystallization and Phase Separation

Weichao Shi,^{†,‡} Jian Yang,[†] Yan Zhang,^{†,‡} Jun Luo,^{†,‡} Yongri Liang,[†] and Charles C. Han^{*,†}

[†]Beijing National Laboratory for Molecular Sciences, Joint Laboratory of Polymer Science and Materials, Institute of Chemistry, Chinese Academy of Sciences, Beijing 100190, China

[‡]Graduate School of the Chinese Academy of Sciences, Beijing 100190, China

ABSTRACT: Crystallization dynamics and lamellar orientation are affected under the dynamic interplay between crystallization and phase separation. We carried out the experiment in a dynamically asymmetric blend of amorphous poly(methyl methacrylate) (PMMA) and crystalline poly(ethylene oxide) (PEO). If phase separation is really weak, lamellae are normally grown in the radial direction within spherulites. Growth rate shows a bell-like curve with respect to temperature. However, when strong phase separation intervenes, the growth rate curve is characterized by double peaks, one of which is dominated by crystallization and the other by phase separation. Meanwhile, lamellae tend to orient in the tangential direction in concentric alternating structures, whose formation mechanism has been explained in previous studies. This lamellar orientation inversion is reflected by a negative to positive birefringence inversion under optical microscopy. Within lamellar stacks, more amorphous molecules tend to be pushed out under the effect of phase separation, leading to smaller long period.



INTRODUCTION

Blending and alloying are important in materials science, in order to meet the multifunctional need in industry.¹ But more than one kind of kinetic mechanisms may be involved mainly due to coupled phase transitions.² Both phase separation and crystallization are often encountered if at least one crystalline component is employed. The dynamics of each individual process has been well studied for many years.^{3–11} However, the mechanism is still a challenge when crystallization and phase separation take place simultaneously. Previously, we investigated phase separation behavior assisted at the growth interface and the concentric structures formed by alternating amorphous-rich and crystalline-rich domains.¹² As phase separation intervenes into the crystallization process, normal spherulitic shape and lamellar orientation may be affected at the same time, depending on the quench depth with respect to the phase boundaries of different transitions involved.

A crystal is always trying to grow after the primary nucleation by regularly arraying crystallizable molecules and rejecting the amorphous ones. In a fully miscible blend, crystalline component usually grows in a spherulitic shape, compact when the majority fraction is crystallizable molecules and loose on the contrary condition.¹³ In some cases, dendritic crystal appears when the crystalline fraction is small.^{14–17} The growth rate with respect to temperature usually show bell-like shape, which is nucleation limited in the high temperature region and diffusion limited in the low temperature region.

Spherulites can be further classified as negative or positive according to the birefringent character. A spherulite with the higher refractive index for light vibrating along the radial direction is called positive. If the higher refractive index is in the tangential direction, a spherulite is called negative. So, macroscopic birefringence may give qualitative information on crystal orientation. There have been a few reports on the presence of both positive and negative spherulites in syndiotactic polystyrene and its blends.^{18,19} Those results indicated that lamellae in spherulites may grow in radial as well as in tangential directions, which led to opposite birefringent properties.

When phase separation intervenes into a crystallization process, the dynamic interplay between these two transitions becomes more complicated. It has been noted in experimental observations^{20–24} that primary nucleation of crystallization can be assisted by concentration fluctuation, especially at the interface boundaries of phase separated domains. Simulation results^{25,26} support the preference of nucleation at the interface, however, without any specific information given on the orientational anisotropy of crystal arrangement.

If glass transition is introduced to mediate the phase transition dynamics, then phase separation is known as viscoelastic phase separation.^{27–29} Compared with normal phase separation, viscoelastic phase separation considers molecular

Received: September 8, 2011

Revised: December 14, 2011

Published: January 5, 2012

relaxation in addition. In this study, we consider the lamellar orientation under the interplay between a crystallization process and a slow viscoelastic phase separation process. One of the advantages of employing such a system is that we are able to mediate the dynamics of the two transitions on a much longer time scale, in contrast to the fast dynamic processes in polyolefin blends. Furthermore, the low mobility of the PMMA-rich phase may fix the regular concentric ring pattern so that lamellar orientation inversion can be observed on a macroscopic scale in alternating PEO-rich phase.

EXPERIMENTAL SECTION

Materials. PMMA was purchased from Aldrich Chemicals with a relative weight-average molecular weight of 15 000 g/mol and polydispersity of 1.73. PEO was purchased from Beijing Chemical Co. with a relative weight-average molecular weight of 20 000 g/mol and polydispersity of 1.08. The molecular weight was determined by gel permeation chromatography. The materials were used after purification. The glass transition temperatures of PMMA and PEO were found to be about +91 and -60 °C, respectively, using a differential scanning calorimeter (DSC, MettlerToledo-822e) at a heating rate of 10 °C/min.

Film Preparation. PMMA and PEO with a given weight fraction were dissolved in chloroform with 5% by weight. The solution was stirred at room temperature over 24 h. The film, with thickness of about 20 μm, was prepared by casting the solution onto a clean glass plate and evaporating the solvent until constant weight in vacuum oven at room temperature. Normally, this took about 24 h. The film sample was prepared independently for each observation. The samples were melted at 130 °C for 30 min for homogenization before each annealing.

Optical Microscopy. The experimental temperature is controlled by a Linkam (LTS350) hot stage. The phase contrast optical microscopy (PCOM) and polarized optical microscopy (POM) are carried out using an Olympus (BX51) optical microscope and Olympus (C-S050ZOOM) camera. The vector direction of the polarizer is kept vertical to the depolarizer. An optical compensating plate, with optical path difference 530 nm, is used to judge the positive or negative birefringence of the spherulites. The compensating plate is inserted in 45° with polarizing elements. The details of the POM instrument used in this study were schematically illustrated in Figure 1. Polarized light

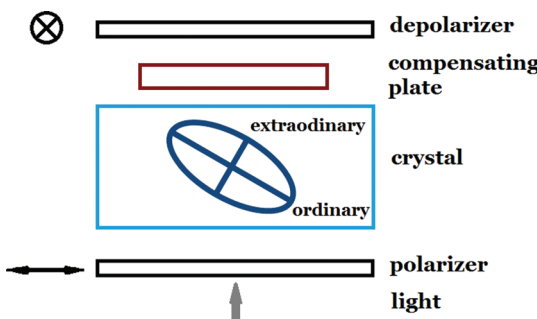


Figure 1. Schematic illustration of the POM instrument used in this study. The axis of the polarizer is parallel to the plane of the paper and the axis of the depolarizer is normal to the plane of the paper (indicated by the cross-in-circle).

with different wavelength have different intensity through the compensating plate. The light at 530 nm completely diminishes. For negative spherulites, the path difference in the I and III quadrants is decreased, showing a yellow color, while the path difference in the II and IV quadrants is enlarged, showing a blue color. The positive spherulites show the opposite property. The isotropic region shows red/purple color.

Scanning Electron Microscopy. Samples were coated by platinum before observation under SEM (JEOL JSM 6700F).

Small Angel X-ray Scattering. The small angle X-ray scattering (SAXS) experiments were performed on a 1.2KW MicroMAX-007HF rotating anode X-ray generator (Rigaku) equipped with a rotating anode Cu target. The X-ray source was operated at 40KV and 30 mA. The wavelength is 0.1545 nm. The diameter of the beam at the sample is about 1.5 mm. All the samples were preannealed on a Linkam (LTS350) hot stage at different temperatures. The SAXS experiments were carried out at room temperature. The transmitted X-ray was stopped by a beam stop and the scattered X-ray was collected by a 2D position sensitive detector.

SAXS Data Analysis. All SAXS scattering data were corrected before analysis by subtracting the background intensity associated with thermal density fluctuations. Following Ruland's approach, the high-q range intensity was fitted by $I(q)q^4 = K_p \exp(-\sigma^2 q^2) + I_B q^4$, where wave vector is $q = 4\pi \sin(\theta/2)/\lambda$ (θ is the scattering angle).^{30,31} K_p is the Porod constant, σ is related to the crystal/amorphous interface, and I_B is the scattering from thermal density fluctuation. The background intensity was subtracted all over the q -range to give corrected intensity $I_C(q)$.

Lorentz correction is generally used in X-ray scattering to correct the scattered intensities ($I_C(q)$) from crystalline materials to obtain correct structure factors, when there is a periodicity with consecutive lamellar structures ($I_S(q)$) in the crystalline systems, following the relationship $I_C(q) = A2\pi/q^2 I_S(q)$.³² So we gave all scattering curves by plotting $I(q)q^2$ versus q . The long periods were calculated directly from the equation $L = 2\pi/q_{max}$, where q_{max} is the wave vector corresponding to the peak maximum in the Lorentz-corrected plots.

The normalized 1D correlation function is defined as

$$g(r) = \int_0^\infty I_C(q)q^2 \cos(qr) dq / Q$$

where $Q = \int_0^\infty I_C(q)q^2 dq$ is the scattering invariant. The intensity at low q (near 0.20 nm⁻¹) and high q (1.3–1.6 nm⁻¹) regions were fitted by Guinier's law and Porod's law, respectively.³³ The thickness of the lamellar crystallites (or the amorphous layer) was obtained by the intersection between the slop of the triangle at $g(r) = 0$ and the horizontal line at the first minimum. The thickness of the lamellar crystal should be larger than that of the amorphous layer, due to the high crystallinity in neat PEO. Because of melting depression, the crystal thickness in the blend should be smaller than that in neat PEO. The crystal thickness in the blend is identified accordingly.

RESULTS AND DISCUSSION

Birefringence and Growth Dynamics. The phase and morphology diagram was given in the previous studies.^{12,34} The binodal line for phase separation locates below the crystal melting line. Accordingly, for a temperature quench, thermodynamic driving force is always larger for crystallization than for phase separation. A dynamic inversion line is also given, which locates deep within spinodal region, for two different reasons. On one hand, phase separation becomes dominant below this inversion line, leading to an inversion from spherulitic to concentric alternating structures.³⁴ On the other hand, lamellar orientation inverts from radial to tangential directions. At shallow quench (region 1 in Figure 2), crystallization dominates the process and negative birefringent spherulites form, with either compact or loose structures. As strong phase separation intervenes into the crystallization process (below the dynamic inversion line, region 2 in Figure 2), positive birefringent concentric ring patterns form.

When PEO weight fraction is over 0.7, compact spherulite always forms in the temperature range in this study. But there is a negative to positive birefringence transition as temperature lowers and PEO content decreases. We will give a detailed

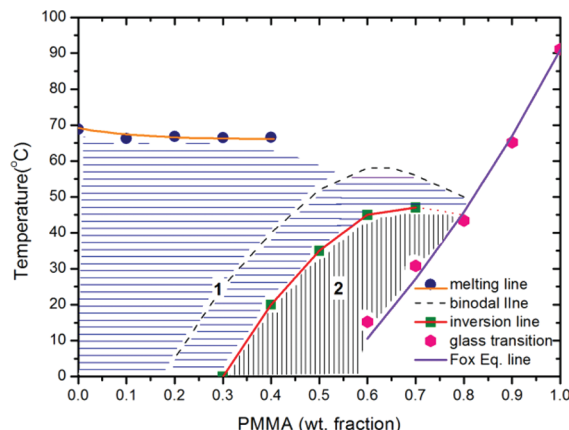


Figure 2. Phase and lamellar orientation diagram of PMMA/PEO blend.¹² Region 1 is crystallization dominated region and region 2 is phase separation dominated region. Lamellae grow in radial direction showing negative birefringence in region 1; lamellae orientation inverts to tangential direction showing positive birefringence in region 2.

discussion on this negative to positive inversion phenomenon below.

When PEO weight fraction is at 0.4, loose negative spherulites form in the temperature range between 45 and 50 °C. At higher temperatures, more compact spherulites grow quite slowly, usually via heterogeneous nucleation on impurities. Below 45 °C, loose spherulites cannot maintain the shape and changes into isolated stacks as phase separation becomes faster with decreasing temperature. Figure 2 shows the typical structure in each region. The characteristic morphologies were observed under PCOM and birefringence under POM.

Parts a and b of Figure 3 show typical spherulitic morphologies above 45 °C, characterized by long fibrillar crystals radiating from the center in the radial direction. The spherulites showed negative birefringent nature. However, Figure 3c shows that loose spherulite broke into short isolated lamellar stacks in phase separated PEO-rich domains, reflecting positive birefringent character macroscopically, when the sample was annealed at 42 °C. As reported in the previous paper,³⁴ the morphology lost the spherulitic shape but inverted to concentric alternating structure below 45 °C, because of effects from phase separation. Here we note that the negative to positive birefringence inversion also occurs near 45 °C. When the

sample was annealed at even lower temperature, lamellar stacks formed in the phase separated domains tended to lose their orientational preference, as shown in Figure 3d. We will give a detailed discussion on the lamellar orientation in the following sections.

As temperature approached glass transition temperature, long-range concentration fluctuation was sharply prohibited. However, after a long time annealing, small negative crystallites appeared again, as shown in Figure 4 where the sample was

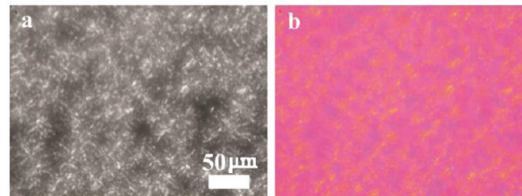


Figure 4. Sample PEO content at 0.4 annealed at 20 °C (near glass transition) observed under (a) POM and (b) POM coupled with a compensating plate.

annealed at 20 °C. To give a short summary, negative spherulites form when phase separation is weak at shallow quench, and invert to positive concentric patterns when phase separation dominates the deep quench region, but finally return to negative spherulites when long-range phase separation is dynamically depressed near glass transition. This also gives additional evidence that positive birefringence originates from phase separation.

As has been illustrated in the previous paper,³⁴ phase separation always grew faster than crystallization, especially below 40 °C. Accordingly, there was always size difference between pictures taken from PCOM and POM at nearly the same time. Measuring growth rate from these pictures taken from the two modes, we can obtain two typical growth rates for phase separated domains and for crystallized areas, respectively. As is shown in Figure 5, there is sharp acceleration of growth rate as temperature is decreasing to below 45 °C until 40 °C, then a mild increase between 40 and 25 °C, and a sharp drop as glass transition (15.2 °C) is approached. The optimum temperature near 40 °C corresponds to the largest growth rate of crystallization in a bell-like growth rate versus temperature curve. Deviations between 40 and 20 °C can be considered that crystallization was assisted in phase separated crystalline-rich domains. The growth peak of phase separation

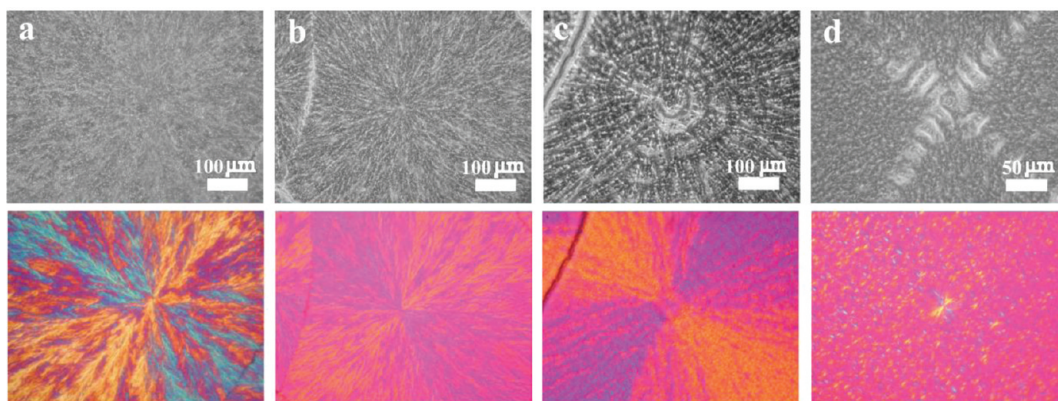


Figure 3. Typical morphology and birefringent character with PEO content at 0.4 annealed at (a) 53 °C, (b) 47 °C, (c) 42 °C, and (d) 30 °C. The pictures in the upper and lower rows were taken under PCOM and POM coupled with a compensating plate, respectively.

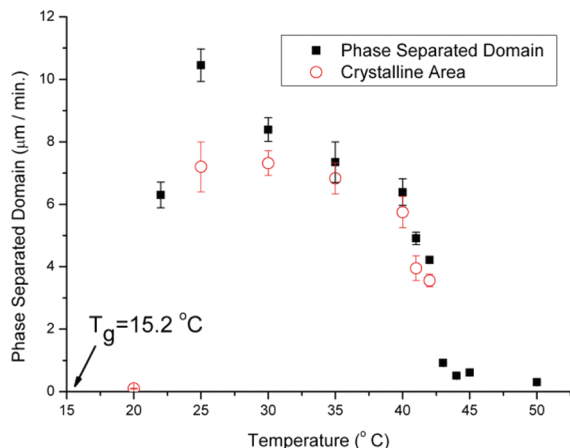


Figure 5. Growth rates of phase separated domains and crystallized areas versus temperature plot for the sample with PEO content at 0.4.

at the lower temperature (near 25 °C) was the result of phase separation with an upper critical solution temperature. So, enlarging quench depth gave larger thermodynamic driving force, and thus accelerated phase separation dynamics. On the other hand, the dynamics was also depressed by slow diffusion when approaching glass transition (below 25 °C).

When PEO weight fraction is at 0.5, compact negative spherulites form above 35 °C. The typical morphology changes to concentric alternating structure below 35 °C, usually with small compact spherulites initiating phase separation at the center. Figure 6 shows the characteristic birefringent pattern observed at different temperatures.

From Figure 6a, we see compact negative spherulites consist of long fibrillar structures. As a larger quench was applied, phase separation intervened. However, phase separation dynamics would not be enhanced significantly until a large enough concentration deviation was built up. This concentration deviation became intensified as the spherulite grew larger. So, as indicated in Figure 6, parts b–d, there were small compact spherulites at the center of the domains. It is interesting to note that the initial spherulites were negative, but the lateral crystallites showed positive nature under the effect of phase separation. This birefringence inversion temperature was measured to be near 35 °C. Also, as coupled with phase separation, short isolated lamellar stacks appeared instead of long fibrils.

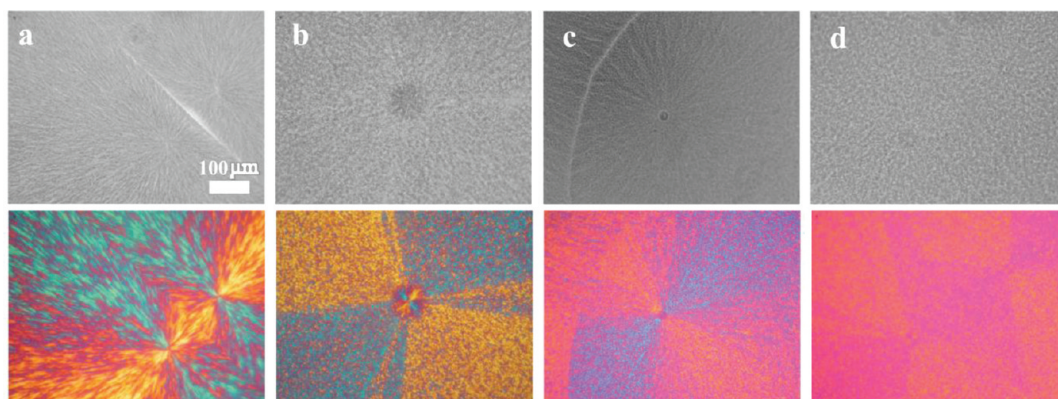


Figure 6. Typical morphology and birefringent character with PEO content at 0.5 annealed at (a) 40 °C, (b) 30 °C, (c) 25 °C, and (d) 20 °C. The pictures in the upper and lower rows were taken under PCOM and POM coupled with a compensating plate, respectively.

The growth dynamics, shown in Figure 7a, is similar to the previously shown sample with PEO content at 0.4. But the

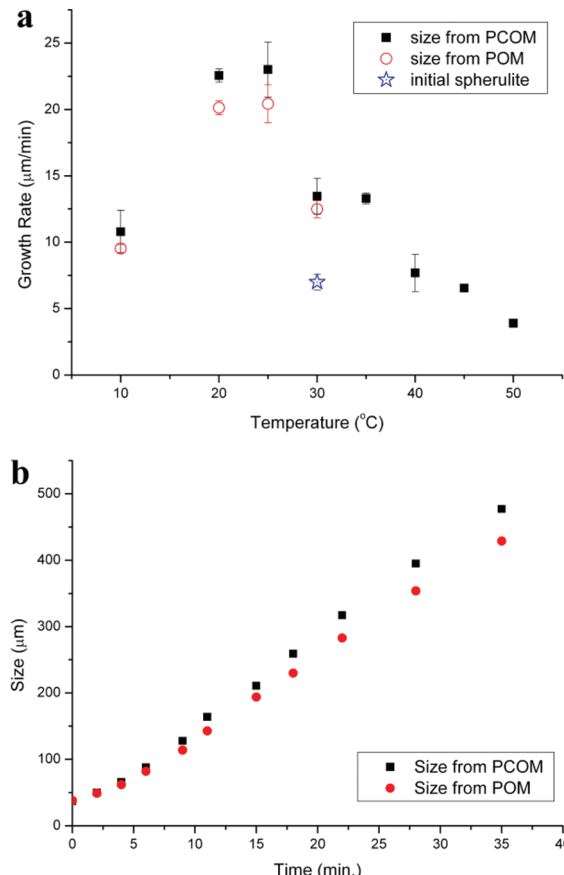


Figure 7. (a) Growth rates of phase separated domains and crystallized areas versus temperature plot for the sample with PEO content at 0.5. (b) Time evolution of the size increment of the sample annealed at 30 °C. Phase separation took place after 5 min.

double peak character (two separated peak temperatures) is more obvious. At higher temperatures between 50 and 35 °C, the growth rate of crystallization increases as temperature decreases. As phase separation intervenes near 35 °C, the growth rate continued to increase as temperature was reduced until near 10 °C. The glass transition temperature is estimated

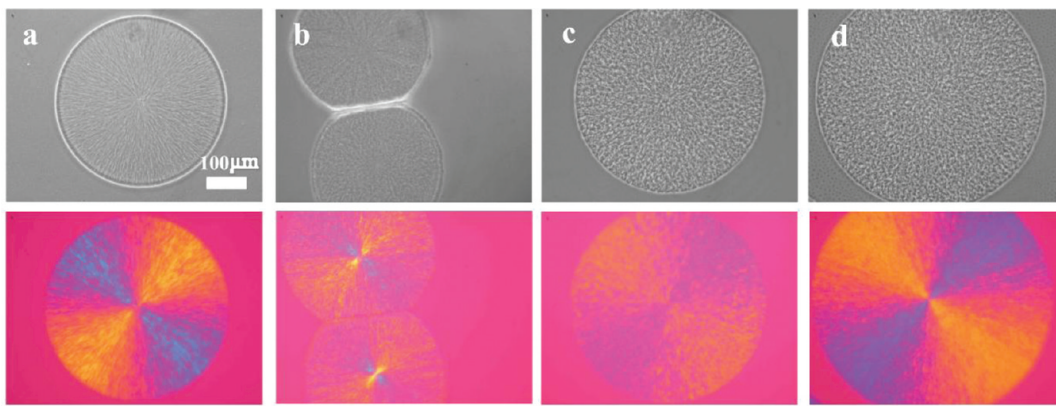


Figure 8. Typical morphology and birefringent character with PEO content at 0.6 annealed at (a) 25 °C, (b) 20 °C, (c) 15 °C, and (d) 10 °C. The pictures in the upper and lower rows were taken under PCOM and POM coupled with a compensating plate, respectively.

to be 0 °C via Fox equation. The melting point should be near 65 °C. So the maximum growth rate of crystallization, in the absence of phase separation, corresponds roughly near 35 °C. This estimation coincides with our experimental results.

As we reported before,^{12,34} crystallization took place first under deep quench, and phase separation occurred at the growth interface of the initial spherulites, and then led to concentric growth of alternating structures. The initial spherulites usually grew to large sizes before phase separation took place, especially shallowly below the inversion line. So we measured the growth rate of the initial spherulites at 30 °C (Figure 7 b), which gave a slow growth rate of about 7.0 μm/min, much slower than the lateral growth under the effect of phase separation. This confirms our estimation above and gives a conclusion, like before, that crystallization dynamics is enhanced by the phase separation at lower temperatures.

Similar birefringence inversion occurs near 20 °C when PEO content increases to 0.6. Compact spherulite showed regular Maltese cross and revealed negative birefringence at 25 °C, as shown in Figure 8a. The negative nature can be still kept at 20 °C. As temperature quench became larger, the structure showed a rough appearance under PCOM and the birefringence inverted to positive nature. The light intensity under POM mode became strong as temperature was decreased more, which reflected that lamellae were arranged more regularly when phase separation dominated the dynamics.

The growth dynamics becomes faster as PEO content increased to 0.6. The glass transition temperature is estimated to be -15 °C via the Fox equation. The melting point should be near 65 °C. So the maximum growth rate corresponds roughly near 25 °C. However, the maximum growth rate appears at a lower temperature near 15 °C. Because of the fast growth dynamics, crystallization occurs in phase separated domains as soon as phase separation takes place under deep quench. This gives the reason for a single peak in Figure 9 and the disappearance of the size difference between pictures under PCOM and POM (Figure 8).

Birefringence inversion occurs near 0 °C when PEO content increased to 0.7. Typical pictures are revealed in Figure 10. Because of the high PEO content, the growth dynamics was too fast (over 100 μm/min) to be precisely determined.

Lamellar Orientation. Birefringence is the consequence of the macroscopic refraction of the lamellae orientation. We will pursue the reason for the birefringence inversion on microscopic/mesoscopic level.

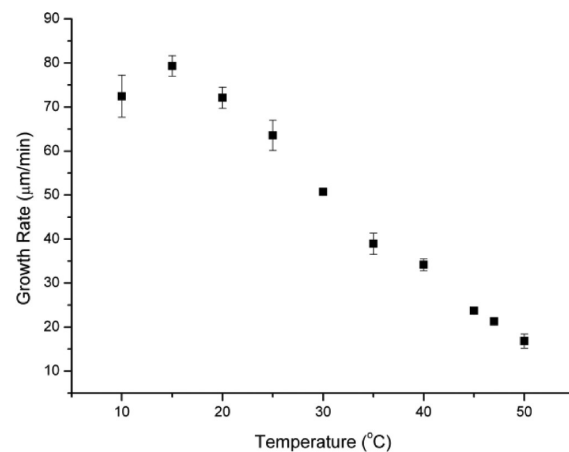


Figure 9. Growth rates of phase separated domains and crystallized areas versus temperature plot for the sample with PEO content at 0.6.

Figure 11a shows the crystal structure under SEM for PEO weight fraction at 0.4 annealed at 47 °C. The sample was etched by tetrahydrofuran (THF). We clearly see the long fibrillar crystals radiating from the center with many short branches, in accordance with Figure 3b. The magnified picture indicates that the lamellae grew in the radial direction, mostly edge-on with respect to the substrate.

Figure 11b shows the crystal morphology for the blend at 42 °C. The etched sample displayed a concentric alternating ring structure, with lamellar stacks oriented perpendicular to the radial direction, in contrast to the radial growth formed at 47 °C. Note that spherulites reflected positive birefringent character at 42 °C, compared with negative nature at 47 °C. Therefore, we may deduce that lamellar orientation inversion affected by phase separation was the origin of the macroscopic birefringence inversion. Unfortunately, it was difficult to observe lamellar structures at even lower temperatures using the etching method because of the isolated distribution of lamellae.

When PEO weight fraction is at 0.5, similar inversion of lamellar orientation can be observed under SEM. Figure 12 shows the typical structures formed at 40, 30, 25 and 10 °C. Above the inversion temperature (35 °C), a compact spherulite formed and long lamellar stripes grew in the radial direction trapping the amorphous domains into the interfibrillar regions. Below the inversion temperature, concentric alternating structures emerged. The lamellae in the crystalline-rich domains

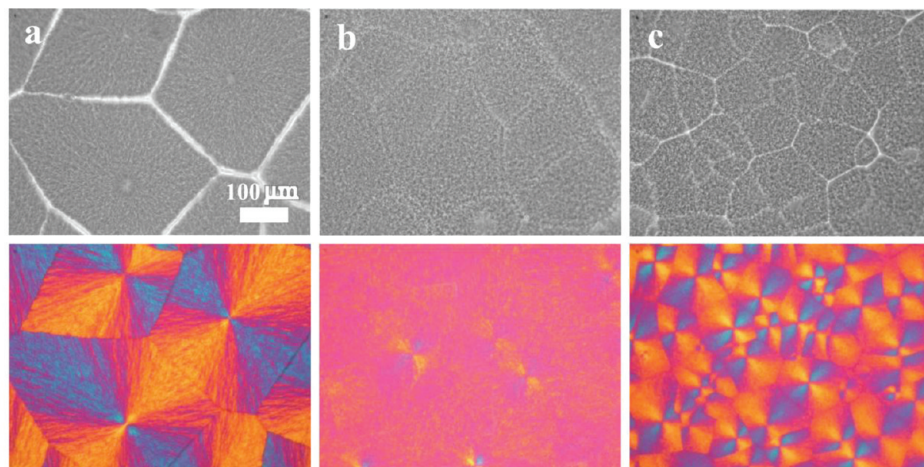


Figure 10. Typical morphology and birefringent character with PEO content at 0.7 annealed at (a) 10 °C, (b) 0 °C and (c) -5 °C.

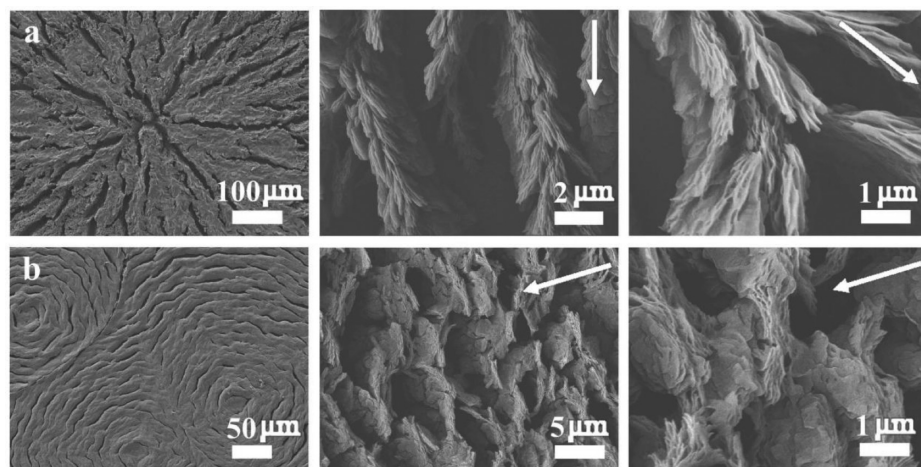


Figure 11. Structure of the sample with PEO content at 0.4 annealed at (a, upper row) 47 °C and (b, lower row) 42 °C observed under SEM after etching by THF. The arrow indicates the radial direction from the center.

tended to orient in the tangential direction. The lamellar arrayed more regularly as the quench depth was enlarged. However, if the regular concentric ring pattern broke up at even lower temperatures, the lamellae in the phase separated domains tended to orient randomly again.

As PEO content increased beyond 0.6, detecting lamellar orientation using etching method became very difficult, because of the compact internal structures formed. Figure 13 shows the typical structures at 25, 15 and 5 °C. Above the inversion temperature (20 °C), the spherulitic pattern was hardly destroyed and compact lamellae still oriented in the radial direction. Below the inversion temperature, in contrast, concentric structure appeared and long lamellar stripes tended to array tangentially.

Characteristic Length from SAXS Data. In this section, we will discuss information on even smaller scale, that is, within the lamellar stacks using SAXS. As a basic concept, thicker lamellae usually formed when crystalline polymer is annealed at shallower quench temperatures. The limiting case is that the thickness should approach infinity as the annealing temperature is approaching the equilibrium melting point. As temperature decreases, the lamellar thickness should decrease because of dynamic and thermodynamic reasons. The distance between

two nearest lamellae, characterized by the long period, reveals important microscopic information. It is known that the contribution to the long period comes from two parts: one is the thickness of lamellae; the other is the amorphous-rich domains in the interlamellar regions. In a fully miscible situation, as the temperature is decreasing or the amorphous component is increasing, the thickness of lamellae decreases but more amorphous molecules may be intercalated into the interlamellar regions.^{30,31} These two opposite factors compete to give the final characteristic length of the long period.

In the neat PEO, the characteristic wave vector, corresponding to the maximum intensity, became larger as temperature was decreased as shown in Figure 14a. The maxima at high wave vectors are the higher order reflections with respect to the low-q maximum. The characteristic long period of lamellar structure decreased from 22.4 nm at 50 °C to 17.6 nm at 10 °C. All samples were annealed for 48 h before scattering measurement. So, we can attribute the thinning trend of lamellae with decreasing temperature mainly to the thermodynamics. However, a similar trend is indicated in Figure 14b when PEO content is 0.6, but the mechanism is distinguishably different as will be discussed later. From the 1D normalized correlation function, as shown in Figure 14c, the detailed lamellar information on

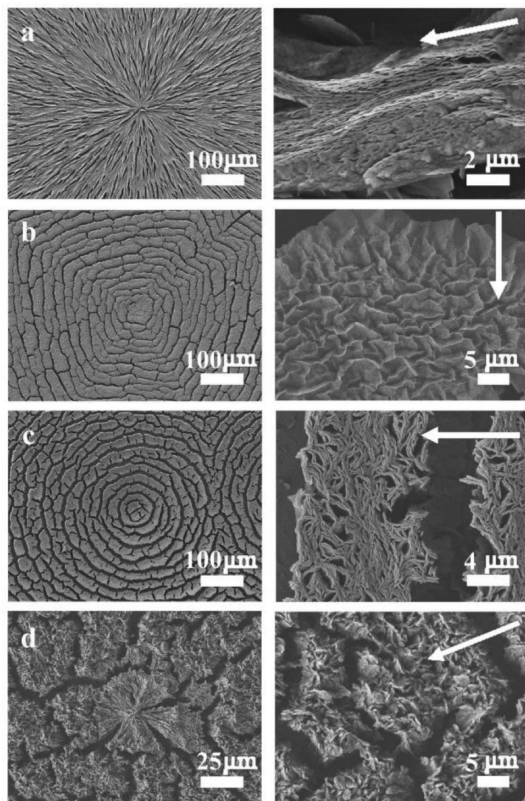


Figure 12. Structure of the sample with PEO content at 0.5 annealed at (a) 40 °C, (b) 30 °C, (c) 25 °C, and (d) 10 °C observed under SEM after etching by xylene (the 40 °C, 30 °C, and 25 °C samples) and THF (10 °C sample), respectively. The arrow indicates the radial direction from the center.

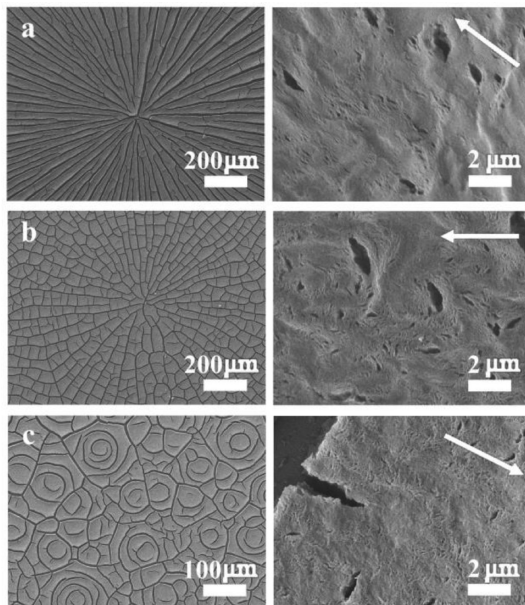


Figure 13. Structure of the sample with PEO content at 0.6 annealed at (a) 25 °C, (b) 15 °C, and (c) 5 °C observed under SEM after etching by xylene. The arrow indicated the radial direction from the center.

the thickness of the crystal and the amorphous layer can be obtained quantitatively.

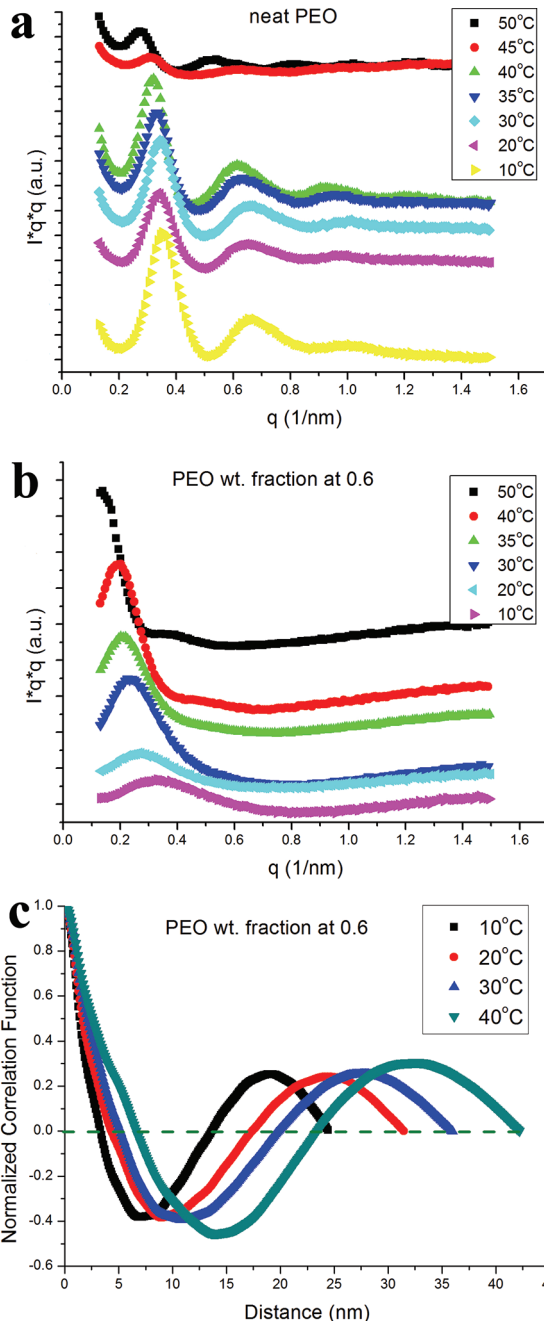


Figure 14. Lorentz-corrected SAXS curves obtained at different crystallization temperatures for (a) neat PEO and (b) PEO content at 0.6. The normalized correlation function for the blend with PEO content at 0.6 is shown in part c.

Figure 15a shows the temperature dependence of the long period for different PEO weight fractions. With respect to the decreasing temperature, the characteristic long period decreased for all compositions. But in the neat PEO, the decreasing trend was small. As the amorphous PMMA content increased, the decreasing trend became larger. Here we compare the lamellar structure in neat PEO and the blend with PEO content at 0.6. The mild dependence of crystal thickness on temperature is shown in Figure 15b. The thickness of the amorphous layer in neat PEO (Figure 15c) is almost unchanged with respect to temperature. For the blend with PEO content at 0.6, however, the thickness of the amorphous

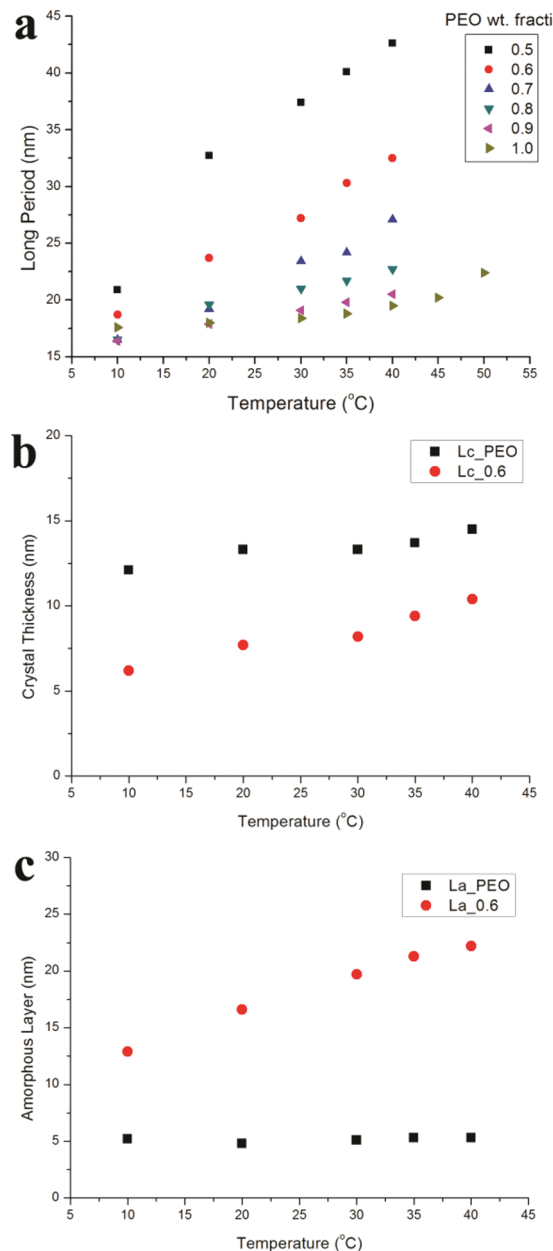


Figure 15. (a) Long period versus temperature plot for the blend. The thickness of the crystal (b) and the amorphous layer (c) with respect to temperature for neat PEO and the blend with PEO content at 0.6.

layer increases drastically as temperature increases. This led to a conclusion that more PMMA molecules were excluded out of the lamellar stacks, beyond the mild decrease of crystal thickness, as temperature decreased mainly due to phase separation.

Figure 16a shows the concentration dependence of the long period change. When samples with different compositions were annealed at the same temperature, the long period increased as more PMMA were involved at temperatures above 20 $^{\circ}$ C. But for temperatures below 20 $^{\circ}$ C, such as samples annealed at 10 $^{\circ}$ C, the long period first decreased slightly and then increased with the increase of PMMA. The monotonic tendency of increased long period at high temperatures indicated that more amorphous PMMA molecules were involved in the interlamellar regions as PEO content decreased. At low temperatures, the amorphous molecules tended to be repelled out by phase separation, accompanied by the decrease of lamellar

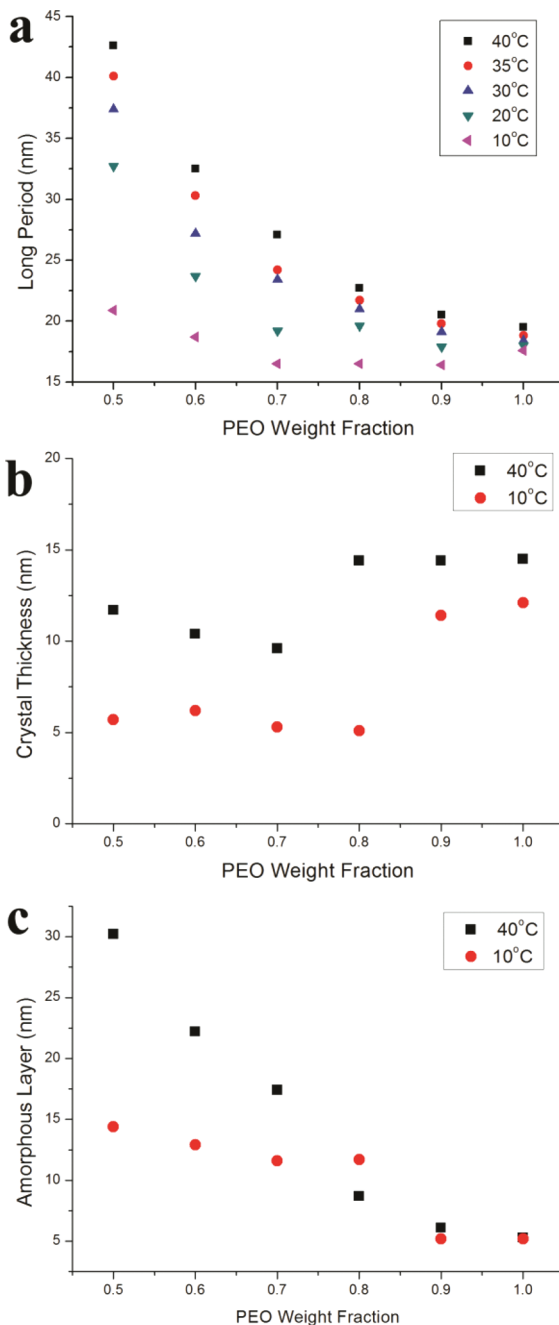


Figure 16. (a) Long period versus PEO weight fraction plot. The thickness of the crystal (b) and the amorphous layer (c) for the blend with different compositions at 40 and 10 $^{\circ}$ C, respectively.

thickness, when a small amount of PMMA was introduced. However, when PMMA content became larger, some amorphous molecules will be trapped in the interlamellar regions, and led to the further increasing of long period. This postulation can be confirmed by analyzing the thickness of the crystal and the amorphous layer obtained from the 1D correlation function, as revealed in Figure 16, parts b and c, respectively. There was minor decrease of the crystal thickness as a few PMMA was introduced. But the crystal thickness dropped drastically over a certain amount of PMMA content, and then increased mildly. The thickness of the amorphous layer increased as more PMMA were introduced into the blend. The increasing tendency was drastic at 40 $^{\circ}$ C but mild at 10 $^{\circ}$ C.

Phase separation tends to occur at lower temperatures below binodal line. On macroscopic scale, this leads to the concentric ring pattern and birefringence inversion. From the above analysis of SAXS results, we may conclude that phase separation may assist the formation of more compact lamellar stacks by pushing the amorphous molecules outward.

Analysis Using Dynamic Competition Model. In our previous papers,^{12,34} we proposed three characteristic times to describe a correlated crystallization and phase separation process. τ_i stands for the induction time for the formation of a new nucleus. τ_d indicates the deformation rate of phase separation. τ_o , the key parameter to correlate the dynamics of crystallization and phase separation, is the diffusion time for the crystallizable molecules crossing over the phase separated domain. Various morphologies are predicted and observed, based on the relative scales of τ_i , τ_o and τ_d .

Furthermore, we would like to define two characteristic time intervals. The first interval, $I_1 = \tau_i - \tau_o$ indexes the relationship between the formation of new secondary nuclei and the original crystal growth. The second interval, $I_2 = \tau_i - \tau_d$ indexes the effect of phase separation on the crystal ordering.

If I_1 is positive, secondary nucleated crystal growth at the original growth front will be the dominant mechanism; the contrary case is, when I_1 is negative, then the crystalline molecules could begin nucleation before reaching the original crystal front and form new crystal, showing aloof tendency. The more negative I_1 is, the less effect was exerted on a new nucleus from the original crystal, which led to a more open structure on a macroscopic scale.

If I_2 is negative, crystallization dominates over phase separation, and crystal growth is hardly affected by phase separation. If I_2 is extremely positive, then crystallization takes place in the well phase separated crystalline-rich domains, like in a homogeneous phase. However, if I_2 is slightly positive, then phase separation could induce directional transport of crystalline molecules that may be fixed by the subsequent crystallization. As phase separation proceeds, molecules should diffuse from one phase, cross an interface and then reach the other phase. This transport process should be normal to the interface, then a coil may preferentially orient in this direction. The lateral crystallization could inherit this orientational preference, and led to lamellar growth parallel to the interface. However, this molecular orientation may be relaxed by thermal fluctuation before crystallization occurs, when I_2 tends to be more positive.

There has been long a debated question: How does phase separation affect crystal ordering? Although a phenomenological postulation was proposed that molecular chains may be deformed and more regularly aligned by mutual (or inter-) diffusion in a phase separation process,^{20,21,23} however, no direct experimental evidence was obtained before. Furthermore, recent simulations did not predict the orientation of lamellar growth under the coupled transitions of crystallization and phase separation.^{25,26} The lamellar orientation inversion reported in this study provides a first direct evidence to confirm that crystal ordering can be affected by phase separation. The failure to obtain a regular array of crystal lamellae in conventional studies (like polyolefin blends), we believe, lies in two factors. One is molecular orientation may be quickly relaxed in dynamically symmetric blends. The other is hydrodynamic coarsening may smear or randomize the possible patterns. But these limitations can be avoided in this dynamically asymmetric PEO/PMMA blend.

Combining the analysis above, we may conclude that the macroscopic birefringence inversion is the result of the microscopic lamellar orientation inversion. In a regular spherulite, negative birefringence means that the refractive index in the tangential direction is larger than that in the radial direction. When concentric ring patterns form, lamellae orient in the tangential directions. Larger refractive index is in the radial direction. Accordingly, concentric ring patterns will have a positive birefringent character. This birefringence inversion is schematically shown in Figure 17.

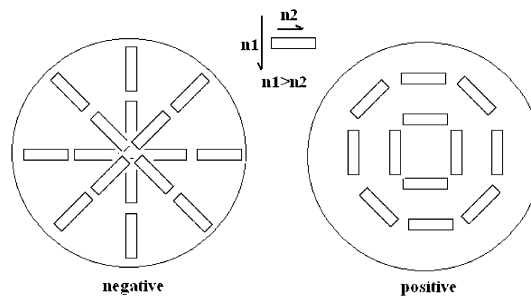


Figure 17. Schematic illustration of the negative birefringence of normal spherulite and the positive birefringence of concentric pattern.

CONCLUSIONS

In this study, a detailed investigation is made on the crystallization dynamics, as well as on the crystal structures at different length scales, under the dynamic interplay between crystallization and phase separation. The growth rate curve tends to show double peaks, in contrast to a bell-like growth rate curve in normal spherulitic growth. Coupled with strong phase separation under deep quench, lamellae prefer to array regularly in the tangential direction, instead of the growth in the radial direction within spherulites. The phase separation effect is also revealed by SAXS within lamellar stacks, reflected by drastic decrease of long period with respect to temperature.

AUTHOR INFORMATION

Corresponding Author

*E-mail: c.c.han@iccas.ac.cn. Telephone: +86 10 82618089. Fax: +86 10 62521519.

ACKNOWLEDGMENTS

This work is supported by National Natural Science Foundation of China (No. 50930003) and the Ministry of Science and Technology of China Special Funds for Innovation in 2009 (2009IM031000).

REFERENCES

- (1) Paul, D. R.; Newman, S. *Polymer blends*; Academic Press: New York, 1978.
- (2) Araki, T.; Qui, T.-C.; Shibayama, M. *Structure and properties of multiphase polymeric materials*; M. Dekker: New York, 1998.
- (3) Flory, P. J. *Principles of polymer chemistry*; Cornell University Press: Ithaca, NY, 1953.
- (4) Onuki, A. *Phase Transition Dynamics*; Cambridge University Press: New York, 2002.
- (5) Cheng, S. Z. D. *Phase transitions in polymers: the role of metastable states*; Elsevier: Boston, MA, 2008.
- (6) Keller, A.; Cheng, S. D. Z. *Polymer* **1998**, *39*, 4461.
- (7) Hoffman, J. D.; Miller, R. *Polymer* **1997**, *38*, 3151.
- (8) Strobl, G. *Rev. Mod. Phys.* **2009**, *81*, 1287.

- (9) Balsara, N. P.; Lin, C. *Phys. Rev. Lett.* **1996**, *77*, 3847.
(10) Hashimoto, T. *Phase Transitions* **1988**, *12*, 47.
(11) Han, C. C.; Akcasu, A. Z. *Annu. Rev. Phys. Chem.* **1992**, *43*, 61.
(12) Shi, W.; Cheng, H.; Chen, F.; Liang, Y.; Xie, X.; Han, C. C. *Macromol. Rapid Commun.* **2011**, *32*, 1886.
(13) Liu, J.; Jungnickel, B.-J. *J. Polym. Sci., Part B: Polym. Phys.* **2007**, *45*, 1917.
(14) Grozhev, N.; Botiz, I.; Reiter, G. *Eur. Phys. J. E* **2008**, *27*, 63.
(15) Ferreiro, V.; Douglas, J. F.; Warren, J.; Karim, A. *Phys. Rev. E* **2002**, *65*, 051606.
(16) Okerberg, B. C.; Marand, H. *J. Mater. Sci.* **2007**, *42*, 4521.
(17) Lorenzo, M. L. D. *Prog. Polym. Sci.* **2003**, *28*, 663.
(18) Wang, C.; Chen, C. C.; Cheng, Y. W.; Liao, W. P.; Wang, M. L. *Polymer* **2002**, *43*, 5271.
(19) Cimmino, S.; Di Pace, E.; Martuscelli, E.; Silvertre, C. *Polymer* **1993**, *34*, 2799.
(20) Zhang, X.; Wang, Z.; Zhang, R.; Han, C. C. *Macromolecules* **2006**, *39*, 9285.
(21) Zhang, X.; Wang, Z.; Muthukumar, M.; Han, C. C. *Macromol. Rapid Commun.* **2005**, *26*, 1285.
(22) Du, J.; Niu, H.; Dong, J. Y.; Dong, X.; Wang, D. J.; He, A.; Han, C. C. *Macromolecules* **2008**, *41*, 1421.
(23) Zhang, X.; Wang, Z.; Dong, X.; Wang, D.; Han, C. C. *J. Chem. Phys.* **2006**, *125*, 024907.
(24) Hong, S.; Zhang, X.; Zhang, R.; Wang, L.; Zhao, J.; Han, C. C. *Macromolecules* **2008**, *41*, 2311.
(25) Mitra, M. K.; Muthukumar, M. *J. Chem. Phys.* **2010**, *132*, 184908.
(26) Ma, Y.; Zha, L.; Hu, W.; Reiter, G.; Han, C. C. *Phys. Rev. E* **2008**, *77*, 061801.
(27) Tanaka, H. *Macromolecules* **1992**, *25*, 6377.
(28) Tanaka, H. *Phys. Rev. Lett.* **1996**, *76*, 787.
(29) Tanaka, H. *J. Phys.: Condens. Matter* **2000**, *12*, R207.
(30) Talibuddin, S.; Wu, L.; Runt, J. *Macromolecules* **1996**, *29*, 7527.
(31) Chen, H. L.; Li, L. J.; Lin, T. L. *Macromolecules* **1998**, *31*, 2255.
(32) Glatter, O.; Kratky, O. *Small Angle X-ray Scattering*; Academic Press: New York, 1982; p 35.
(33) Strobl, G. *The Physics of Polymers*, 2nd ed.; Springer: New York, 1978; p 151.
(34) Shi, W.; Han, C. C. *Macromolecules* **2011**, DOI: 10.1021/ma201940m.